CrossMark

A Study of Water-Inrush Mechanisms Based on Geo-Mechanical Analysis and an In-situ Groundwater Investigation in the Zhongguan Iron Mine, China

Wenhao Shi[1] · Tianhong Yang[1] · Qinglei Yu[1] · Yang Li[1] · Honglei Liu[1] ·
Yongchuan Zhao[1]

Abstract The Zhongguan iron mine is strongly threatened by water inrushes because of the thick Ordovician limestone aquifer and a variety of concealed faults. An inrush event occurred at −260 m below sea level (bsl), inundating the mine during the mineral deposit developing stage. It was very important to understand why and how this occurred to prevent its recurrence. A numerical simulation of a process-based model of the excavation, together with an in-situ groundwater investigation, showed that the event was related to the normally impermeable X1 fault, which was gradually activated from the bottom of the aquifer to the mine roof as excavation developed. The activated fault transformed into an inrush channel, hydraulically connecting the aquifer and the roadway. Thus, faults and other geological structures have to be mapped before mining. Moreover, sealing possible water channels before excavation in potential inrush areas is much better than advance dewatering because of the aquifer's transmissivity and the limited effectiveness of grout curtains.

Keywords Fault · Groundwater level · Ordovician limestone · Grout curtain · Excavation · Numerical simulation

✉ Wenhao Shi
swh601@126.com

✉ Tianhong Yang
yangtianhong@mail.neu.edu.cn

1   Key Laboratory of Ministry of Education on Safe Mining
    of Deep Metal Mines and School of Resources and Civil
    Engineering, Northeastern University, Shenyang,
    Liaoning 110819, China

Introduction

Mining-induced groundwater inrushes have caused grievous casualties and heavy economic losses in mines in China, and can also seriously affect the geohydrological environment. Therefore, it is vitally important to know when, where, and how groundwater inrushes can occur during the mining process (Donnelly 2006; Li et al. 2011; Yang et al. 2007; Zhang et al. 2009; Zhang and Shen 2004; Zhu and Wei 2011; Zuo et al. 2009).

The three main types of mine water disasters in China are: (1) water inrushes from the Cenozoic loose-rock porous aquifer; (2) water inrush from bedrock fissure aquifers; and (3) water inrush from the Ordovician limestone aquifer (Wu et al. 2013; Yin et al. 2015; Zhang and Shen 2004). The last of these is the most serious and occurs where the Ordovician limestone aquifer lies under Permo-Carboniferous coal seams (Zhang 2005), because the limestone is a confined karst aquifer that receives abundant recharge where it outcrops and maintains very high water pressures (Wu et al. 2013; Yin et al. 2015). In northern China, over 130 mines are threatened by water inrushes from the Ordovician aquifer (Li and Zhou 2006). This includes the world's largest water inrush, which occurred in the Fangezhuang coal mine, in which the maximum water inflow reached 2053 m^3/min, submerging the mine and three other nearby mines in less than a day (Yin and Zhang 2005).

The water-inrush channel is as important as the water source to understand the cause and mechanism of a water-inrush incident. Water-inrush channels can be divided into two main types: natural ones, such as karst collapse pillars (KCPs) (Ma et al. 2015; Yin et al. 2004; Zhu and Wei 2011) and faults (Li et al. 2011; Zhang et al. 2014; Zhu and Wei 2011) and mining-related channels, such as roof-caving

⚫ Springer

induced fissures zones (Feng et al. 2007; Sun et al. 2009), floor-stress induced broken zones (Shen et al. 2015; Yang et al. 2007), and poorly plugged boreholes (Wang et al. 2009; Zhang et al. 2015). More than 80% of mine water inrush accidents in underground coal mines are related to faults (Li et al. 1996; Wang and Miao 2006). Thus, fault activity is an important key factor in determining the safety of mine construction and mining. The Zhongguan iron mine, in northern China, has been strongly threatened by water inrushes because of the thick Ordovician limestone aquifer and various concealed faults in the area.

In recent decades, many water-inrush incidents have been researched to explain their underlying mechanisms, so that effective engineering-remedial measures can be developed to prevent the same incident from occurring again (Feng et al. 2007; He et al. 2011; Li et al. 2013; Sun et al. 2009). Thus, it was important to study the water-inrush incident in the Zhongguan iron mine that occurred on Sept. 27, 2013, during the mineral deposit developing stage. Both an in-situ groundwater investigation and a numerical simulation of the event was carried out to better understand the mechanism of this water inrush, so that we can mitigate similar hazards during future mining.

## Background of Geologic Conditions and Study Site

Engineering Background and Natural Setting

The Zhongguan mine is located within Zhongguan village of Shahe city, Hebei province, in north China, 36°55′N longitude and 114°01′E latitude, covering an area of approximately 1.2 km^2. The mine area's elevation ranges from 200 to 270 m above sea level (asl). It has a continental monsoon climate, with warm temperatures and clear cut seasons. The annual average precipitation is about 540 mm. Geological exploration of the area was completed by the No. 2 Geological Party of Hebei province in 1974. However, the iron ore was not mined until 2008 due to the Ordovician limestone's extremely rich groundwater supply. In recent decades, much of this groundwater has been pumped for irrigation, industry, and household consumption, lowering the water table in the area by 156 m, which has provided improved mining conditions. Groundwater levels ranged from −5 to −20 m below sea level (bsl) in Feb 2016; the aquifer thickness is about 200 m.

The latest supplementary geological exploration was finished by the North China Engineering Investigation Institute Limited Company in 2007. According to their geological report, the strata of the area are, successively: the Quaternary Holocene, a Permian formation of interbedded sandstone and shale, a hardly explored Upper Paleozoic Carboniferous formation, the Lower Paleozoic Ordovician limestone, and a Yanshanian formation altered diorite. The mineral deposit is a magnetite ore body of contact-metasomatic skarn, which occurs where the Yanshanian diorite contacts the Ordovician limestone, and is mostly surrounded by the altered diorite. The strata of the Zhongguan iron mine is shown in Fig. 1. The main aquifer flooding potential is associated with the Ordovician limestone, which is thickly bedded and dolomitic. The limestone roof ranges from 80 to 180 m asl The aquifer is called the Ordovician limestone-unconfined aquifer and is recharged by rainfall. The flow direction is from the northwest to southeast, with a hydraulic gradient of only 0.4%.

Fig. 1 Southwest perspective on the stratum structure of the Zhongguan iron mine
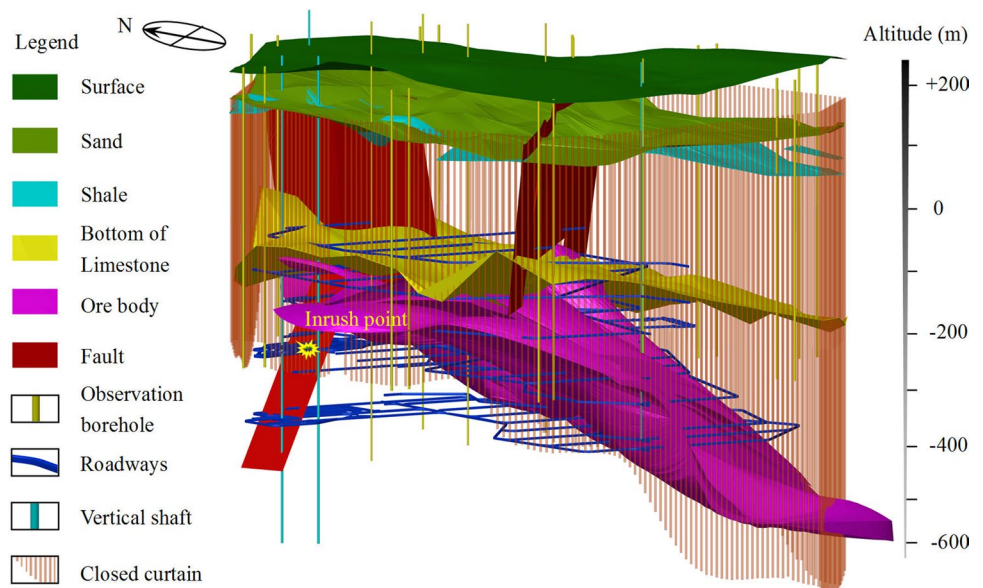
Study Site

The study site is at −260 m bsl, near the main and auxiliary shafts in the northwest of the mine. A serious water-inrush incident occurred at the central substation, 20 m from the east connection roadway. Before the incident, a water inflow of 10 m^3/h was estimated based on advance water detection. However, when the face was advanced 7 m from Sep 7 to 12, 2013, the normal X1 fault, with a dip direction of about 280° and a dip angle about 67°, was gradually exposed in the roof, floor, and ribs of the roadway. Fault gouge extended up to about 45 m from an area immediately adjacent to the roof of the roadway. A wedge-shaped roof collapse about 5 m in height occurred around the fault during the excavation, while roof water leakage gradually worsened, from 35 to 100 m^3/h. A concrete water-retaining wall was built in an attempt to prevent water inflow into the roadway, but it failed. Then, when a second, greater, roof collapse occurred on Sept. 26, the water inflow suddenly increased to 480 m^3/h. The incomplete wall was destroyed and the roadway, with a volume of about 10^4 m^3, were finally inundated on Sept 27, 2013.

Analysis of the In-situ Groundwater Investigation

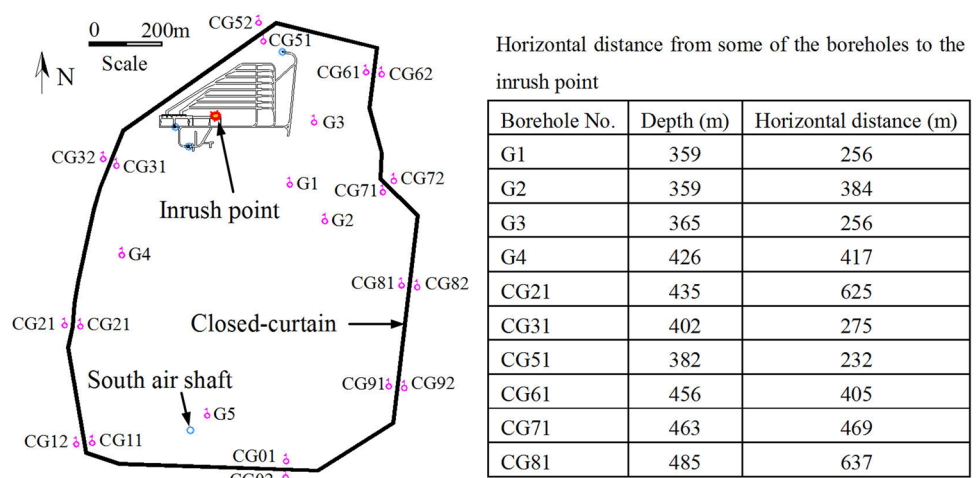### In-situ Observations of Groundwater Levels in Boreholes

A closed boundary grout curtain was constructed in July 2010 by partitioned grouting, with a 30 m per step grouting depth (Bai et al. 2008), in an attempt to prevent groundwater from flowing into the mine area. The top of the grouting holes were all about 100 m asl, and the holes extended into the Yanshannian diorite, with a depth ranging from 321 to 810 m. The final diameter of the holes were 91 mm. The curtain was about 3.4 km in circumference and contained 270 grouting holes. It was anticipated the completed grout curtain would exclude about 80% of the water; however, it was, in fact, much less effective than that. There were five boreholes, numbered G1–G5, in the mine area, and nine pairs of boreholes located just inside and outside of the closed curtain (Fig. 2). These holes were used for groundwater level measurements prior to and during mining.
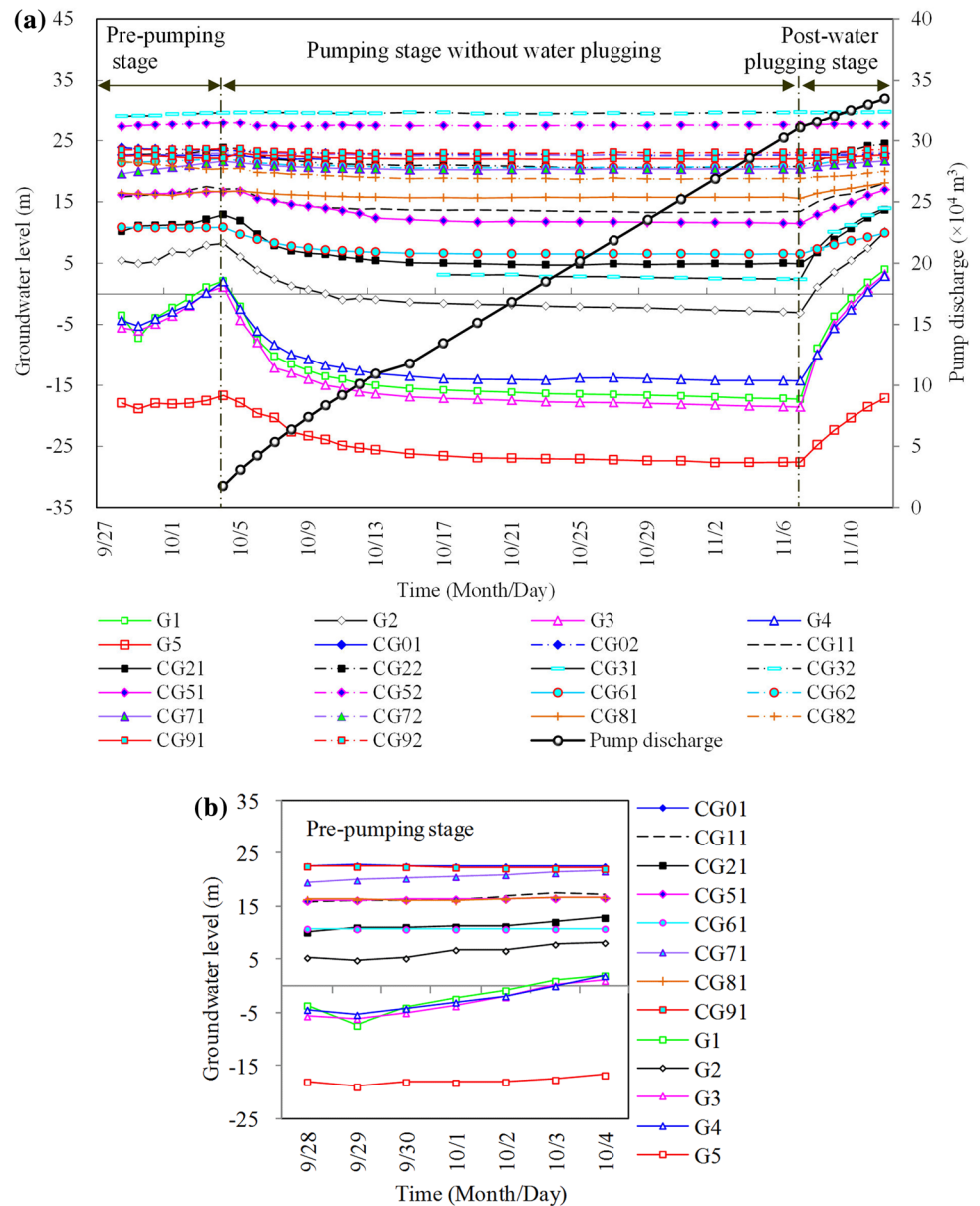
Determination of the Water-inrush Source

Before the fault was exposed on Sept. 7, water inflow near the working face was steady, at an inflow rate of about 10 m^3/h, as mentioned above. No water source that could cause this incident was found by the advance boreholes, although they went through the X1 fault. Figure 3 gives the observed results of groundwater in the mine area after the water-inrush incident on Sept. 27, 2013. The groundwater levels changed in three stages, i.e., the pre-pumping stage from Sep 27 to Oct 4, the pumping stage without water plugging from Oct 4 to Nov 7, and the post-water plugging stage after Nov 7 (Fig. 3a). It is a remarkable fact that the water levels observed in boreholes G1–G4 all rose to different degrees, rather than lowering with time, in the pre-pumping stage. Water in boreholes near the inside of the curtain either remained steady or had a small rise (Fig. 3b). It is known that a cone of groundwater depression had formed in the area before the water-inrush incident. If the groundwater inside the closed curtain was sealed and did not have enough recharge, groundwater levels close to the inside of the curtain would lower more or less with groundwater flowing into roadways, when the water inrush occurred. This observation shows that the groundwater in the closed curtain was not sealed and could be easily recharged from the outside. When water recharge from outside of the curtain exceeded water inflow into the roadways, groundwater inside the curtain should have risen, with the

Fig. 2 Observation boreholes for groundwater levels in the mine area

Horizontal distance from some of the boreholes to the inrush point

Borehole No.	Depth (m)	Horizontal distance (m)
G1	359	256
G2	359	384
G3	365	256
G4	426	417
CG21	435	625
CG31	402	275
CG51	382	232
CG61	456	405
CG71	463	469
CG81	485	637

Fig. 3 a Changes in groundwater levels at different boreholes and pump discharges from Sep 27 to Nov 13, 2013; **b** groundwater level monitoring *curves* at the boreholes inside the curtain from Sep 27 to Oct 4, 2013 (*Note* no indication of broken boreholes at CG12 and CG31 can be observed before Oct 17)

Water Recharge

As shown in Fig. 3a, when water was pumped from the main and auxiliary shafts on Oct 4, groundwater levels in boreholes G1–G4, close to the shafts, were observed to decline rapidly, i.e., the maximum drawdown rate was up to 29 cm/h in boreholes G3 and G4, 23 cm/h in borehole G1, and 16 cm/h in borehole G2. This shows that the hydraulic connection of the Ordovician limestone was very strong.

cone of groundwater depression rising gradually, as was observed in boreholes G1–G4 (Fig. 3b). This indicates that the water-inrush sources were static water inside the closed curtain and dynamic outside.

The total pump discharge was about 9×10^4 m³ from Oct 4 to 11. After that, the pump discharge averaged about 350 m³/h, almost equal to the water inflow, so groundwater levels in the mine area showed a stable and very slow decline. When the inrush point was plugged on Oct 7, groundwater levels in the mine area reached the same level as when pumping began in just 3 days. This once again verified the strong hydraulic connection of the Ordovician limestone groundwater and the rich water recharge outside of the curtain.

Figure 4 shows the groundwater level in each pair of boreholes on Oct 4 and Nov 7, 2013. The maximum water level difference between boreholes CG32 and CG31 was 27 m, with about 16 m between boreholes CG52 and CG51. The groundwater levels in boreholes CG32
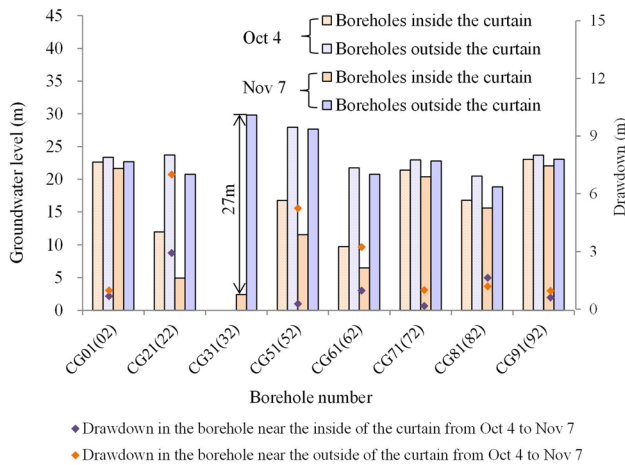
Fig. 4 Comparison of groundwater levels in each pair of boreholes on Oct 4 and Nov 7, 2013

and CG52 remained the same (Fig. 3a), indicating that the northwest curtain was effective. However, the quality of the curtain around boreholes CG22 and CG62 was not as good, for although the water levels were the same in the two paired boreholes, this was because of their synchronous decline. Therefore, groundwater northeast and southwest of the mine area outside of the curtain was the major dynamic water recharge source. Groundwater levels in the two pairs of boreholes, i.e. CG71 and CG72, CG81 and CG82, located downgradient of the mine, showed the same, but less obvious trends. Water-level changes in the other three pairs of boreholes located south of the curtain were mainly affected by pumping from the south air shaft. Hence, groundwater from east of the mine area outside of the curtain is a minor source of dynamic water recharge. Water recharge from outside of the curtain was not sufficiently stopped by the closed grout curtain.

Mechanism of Fault-controlled Water-inrush Induced by Excavation

Effective Stress Equation

Mechanical behavior analysis, without considering seepage, was not suitable for the Zhongguan mine, which contains large amounts of groundwater. Therefore, effective stress, combining applied stress and pore fluid pressures, was used for porous rock mass mechanical analysis, based on the continuum medium model. The mechanical constitutive equation for steady state behavior can be defined as:

$$\sigma'_{ij} = \sigma_{ij} - \alpha p \delta_{ij}, \tag{1}$$

and the seepage equation is defined as:

$$K\nabla^2 p = 0, \tag{2}$$

where σ'_{ij} and σ_{ij} is effective and total stress tensor, respectivly, p is porous pressure, K is hydraulic conductivity, $\alpha(\leq 1)$ is Boit's effective stress coefficient, and δ_{ij} is the Kronecker symbol. The failure criterion chosen for the model was the Mohr–Coulomb failure model, which has been widely used in geotechnical engineering to predict rock mass failure (Li et al. 2011; Ma et al. 2015; Yang et al. 2007; Zhu and Wei 2011).

A simplified finite element numerical model, which accounts for the effects of seepage, was constructed to simulate the effect of the excavation process on stress and damage distribution. The model was solved using COMSOL Multiphysics (COMSOL 2008), a powerful PDE-based multiphysics modeling environment, wherein the boundary and initial conditions are specified (Zhu and Wei 2011).

Numerical Model

Based on the geological, geomechanical, and hydrogeological data, a simple numerical model that incorporated fault X1, was constructed according to plan strain conditions. The model was 350 m long and 350 m high, with a depth ranging from 0 to −350 m bsl, and contained two rock strata (Fig. 5a). The groundwater level in the area was about 0 before the water inrush incident in Sept, 2013, so the hydraulic pressure in the upper Ordovician limestone layer was about 2.2 MPa. The lower diorite would have sustained the water pressure if the fault did not exist, and therefore was considered a protective layer. The roadway located at −260 m bsl was surrounded by the diorite. As mentioned above, the X1 fault zone, which is filled with soft-rheology-plastic fault gouge, breccia and altered diorite, was viewed as a weak zone.

For the mechanics analysis, the external boundary stress of 5.2 MPa in the y direction σ_y was applied at the top surface to be equivalent to the overburden strata weight, while zero displacement was imposed at the left and right sides and base of the model. For the seepage boundary conditions, a constant hydraulic head of 220 m was applied at the top, left, and right sides of the limestone strata. At the boundary of working face, a pressure of 0.1 MPa was applied to simulate atmospheric pressure (Zhu and Wei 2011). A Newman boundary condition with zero flux was applied at the external boundary of the diorite strata.

The rock strata and fault were assumed to be homogeneous and isotropic during the finite element analysis based on COMSOL Multiphysics (COMSOL 2008). The mechanical properties of the rock mass used in the numerical simulation (Table 1) were empirically estimated and

Fig. 5 a Numerical model setup for studying the water inrush induced by the excavation; **b** detailed view of the roadway excavation

(a)

(b)
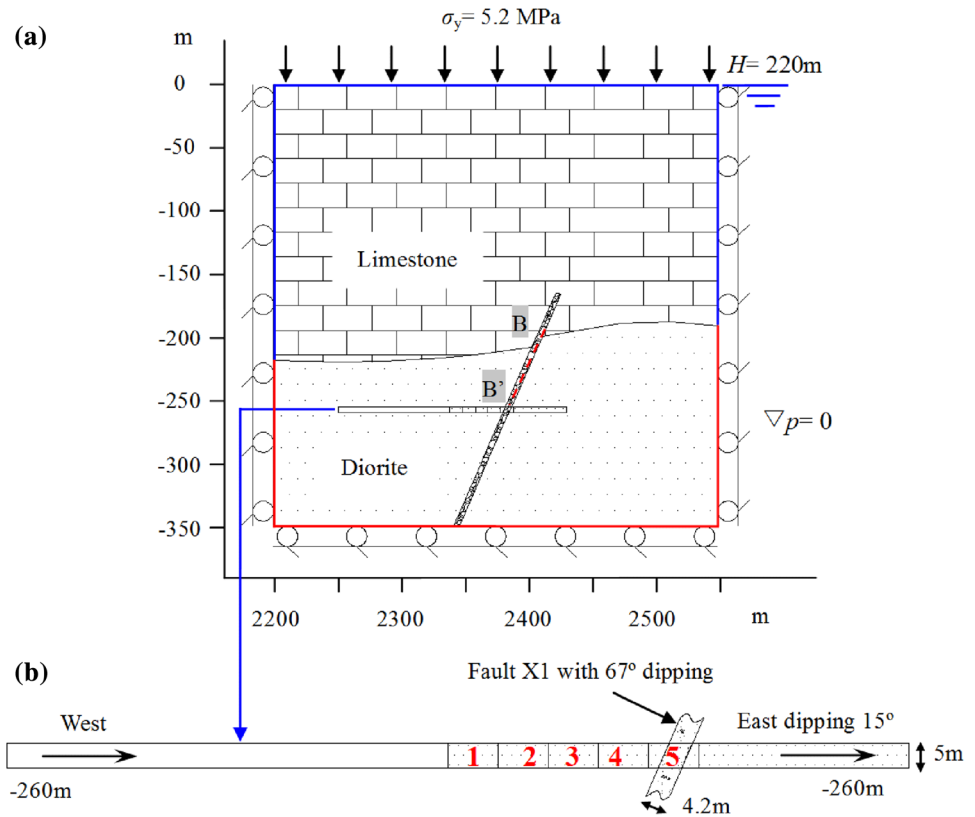
Table 1 Physico-mechanical parameters of rock masses obtained using the RMR system in association with previous engineering experiences

Stratum	Density	Tensile strength	Deformation parameters		Mohr–Coulomb parameters		Hydraulic conductivity	Biot's coefficient α
	ρ (kg/m^3)	σ_t (MPa)	E (GPa)	μ	c (MPa)	φ (°)	K (10^{-7} m/s)	
Limestone	2670	1.4	7.6	0.24	5.3	37	2300	1
Diorite	2780	1.8	8.3	0.22	6.5	43	5.8	0.01
Fault	2260	0.1	1.0	0.3	1.2	27	10	0.1

calibrated in accordance with the RMR classification system (Xia 2014; Zhu and Wei 2011).

Mechanism of the Formation of the Water-inrush Channel

In the following section, we describe the progressive evolution of the water-inrush channel during a five-step excavation sequence with an advance increment of 10 m/step (Fig. 5b). Figure 6 shows the shear stress and damage zone distribution at different simulation steps. In these figures, the black colors denote the damaged zone. Figure 7 shows the stress and displacement distribution of the center profile of the upper part of fault X1 from −195 to −255 m bsl (see profile BB' in Fig. 5a) during the excavation.

As mining advanced, damage zone development in the fault and its broken area strongly depended on the excavation activities. We used evolution of the damage zone as an index to visualize the evolution of the failure zones, which were the path for groundwater in the developing outburst structure.

With the first excavation to 10 m from the left boundary, 35 m from the center of the fault, a small amount of damage occurred in the lower part of the fault, while no damage occurred in the upper part (Fig. 6b). Therefore, the fault was still stable even through the maximum displacement at the upper part of the fault has reached 7.0 mm (Fig. 7c). When the working face was extended to 20 m (second step), the maximal shear stress of the fault at −209 m bsl was 2.44 MPa, with a vertical height of 46 m from the roof (Fig. 7a). Under this ground stress and pore pressure, a small amount of damage of the upper part of the fault

Fig. 6 Shear stress of the model and formation process of water-inrush channel induced by the excavation according to the damage zone (Unit: MPa): **a** damage zone before the excavation; **b** damage zone at excavation step 1; **c** damage zone at excavation step 2; **d** damage zone at excavation step 3; **e** damage zone and detailed view of the fault at excavation step 4; **f** damage zone at excavation step 5
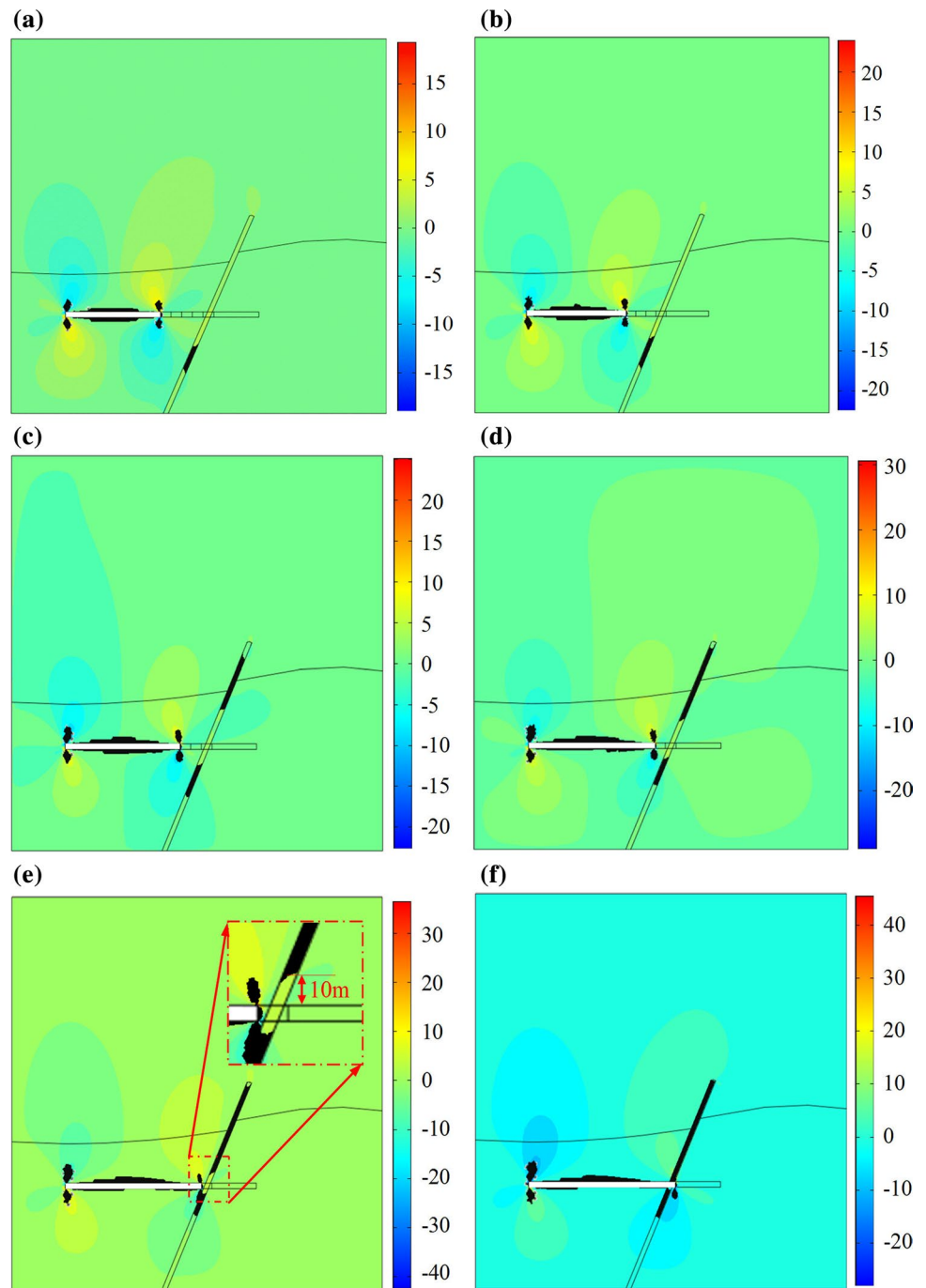
first occurred at the junction of the limestone and diorite (Fig. 6c), causing groundwater in the limestone to flow into the fault's failure zone, increasing the relative hydraulic head of the roof.

When the working face was extended to 30 m (third step), the maximal shear stress of the upper part of the fault still occurred at −209 m bsl, but it increased to 2.86 MPa, with a growth rate of 17.2% (Fig. 7a). The damage zone extended both upwards and downwards compared to the second step (Fig. 6d).

When the working face was extended to 40 m (fourth step), 5 m away from the fault center, a maximal shear stress of 3.75 MPa occurred at −234 m bsl, with a vertical height of 21 m from the roof (Fig. 7a). Meanwhile, part of the minor principal stress in the upper part of the fault changed from compressive stress to tensile stress (Fig. 7b), destabilizing the fault due to the no-tension property of the fault, and increasing groundwater flow into the fault. The damage zone expansion in the upper part of the fault kept the same trend as in the third step,
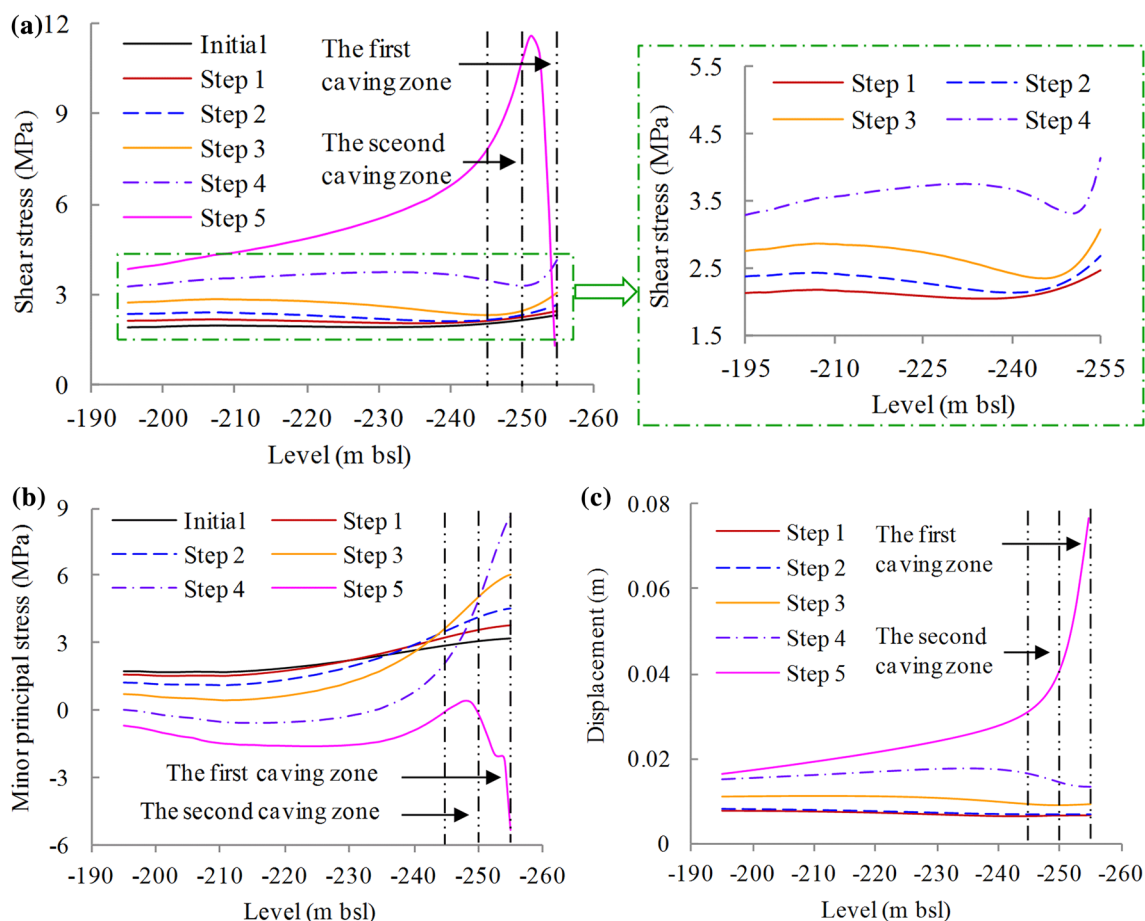
Fig. 7 Stress and displacement distribution of the profile BB' in fault X1 during the excavation **a** shear stress, **b** minor principal stress; **c** displacement

and the damaged zone was about 10 m from the roof (Fig. 6e). Consequently, this 10 m high part of the fault was still stable and could prevent groundwater from flowing into the roadway, mining had not advanced further. That was confirmed by the advance boreholes, as already mentioned.

When the working face extended to 50 m, the fault was completely exposed. The maximum shear stress at −252 bsl, 3 m above the roof, increased sharply, to 11.6 MPa (Fig. 7a). The most upper part of the fault was in tension and the maximum tensile stress at the roof was 5.35 MPa, much more than the tensile strength (Fig. 7b). The roof was displaced by as much as 76.4 mm downward, due to the fault extraction (Fig. 7c). Consequently, the last 5 m of the fault collapsed under the concentrated high shear and tensile stress, causing a wedge-shaped roof collapse, and fully damaging the upper part of the fault, establishing the hydraulic connection between the limestone and the roadway (Fig. 6f). This allowed groundwater from the limestone to flow through the fault, washing out the arenaceous and pelitic karstic deposits, leading to a less obstructed flow

channel. With the second roof collapse, the channel was completely formed and the groundwater outburst occurred.

Conclusions

An in-situ groundwater investigation and a numerical simulation of a process-based model for the excavation were analyzed to study the water-inrush incident in the Zhongguan iron mine. The main conclusions were:

1. The closed grout curtain was incapable of blocking the water because of the strong hydraulic connection of groundwater in the limestone. Groundwater from inside the curtain burst into the roadway and was recharged rapidly from the outside. Therefore, both the static reserves inside the curtain and the dynamic reserves outside the curtain were water sources. Groundwater from northeast and southwest of the curtain was the major dynamic water recharge source, while flow from east of the curtain was minor.

2. A simulated evolution of the damage zone in fault X1 revealed the water inrush development process. The damaged zone in the fault extended downward gradually from the bottom of the aquifer to the roof, as the working face advanced to the fault center. When the face passed fault X1, the fault was fully damaged, creating a channel for the water outburst. Thus, the water-inrush incident was the result of the advancing damaged zone, and hence, the damaged zone in the fault can be seen as a predictor for water-inrush through faults.

3. The water-inrush incident has shown that a naturally impermeable fault can be changed into a water-inrush channel by mining. Therefore, it is critically important to detect and map faults and other geological structures with poor mechanical properties before excavation, whether they are hydrous or not. Also, if a fault is identified as water-free by a horizontal cover hole before excavation, more acclivitous cover holes should be drilled to probe for inflow from higher positions of the fault for further confirmation, 10 m above the roof or even higher.

References

Bai JB, Xu BQ, Zhou HF, Li XB (2008) Mine curtain grouting and its effect testing. Metal Mine 383(5):83–85

COMSOL AB (2008) COMSOL Multiphysics version 3.5a, User's guide and reference guide. http://www.comsol.com

Donnelly LJ (2006) A review of coal mining induced fault reactivation in Great Britain. Q J Eng Geol Hydroge 39(1):5–50

Feng QY, Zhou L, Yang TH (2007) A case study of rock failure and water inrush from the coal seam roof. J Min Safety Eng 24(1):17–21

He KQ, Yu WC, Jiang WF (2011) Analysis of groundwater inrush conditions and critical inspection parameters at the Baixiangshan iron mine, China. Mine Water Environ 30(4):274–283

Li GY, Zhou WF (2006) Impact of karst water on coal mining in north China. Eng Geol 49(3):449–457

Li LJ, Qian MG, Li SG (1996) Analysis of water inrush induced by faults. J China Coal Soc 21(2):119–123

Li LC, Yang TH, Liang ZZ, Zhu WC, Tang CA (2011) Numerical investigation of groundwater outbursts near faults in underground coal mines. Int J Coal Geol 85:276–288

Li T, Mei TT, Sun XB, Lv YG, Sheng JQ, Cai M (2013) A study on a water-inrush incident at Laohutai coalmine. Int J Rock Mech Min 59(2):151–159

Ma D, Bai HB, Wang YM (2015) Mechanical behavior of a coal seam penetrated by a karst collapse pillar: mining-induced groundwater inrush risk. Nat Hazards 75(3):2137–2151

Shen RX, Qiu LM, Li BL, Kong B, Niu Y (2015) "Three fields" evolution of water inrush process under high confined water in stope floor. J Min Safety Eng 32(2):213–218

Sun YJ, Xu ZM, Dong QH (2009) Monitoring and simulation research on development of water flowing fractures for coal mining under Xiaolangdi reservoir. Chin J Rock Mech Eng 28(2):238–245

Wang LG, Miao XX (2006) Numerical simulation of coal floor fault activation influenced by mining. J China Univ Min Technol 16(4):385–388

Wang JC, Xu YC, Yue ZC (2009) Mechanism and treatment method for potential water leakage of aquifer through boreholes in Ordovician limestone. Chin J Rock Mech Eng 28(2):342–347

Wu Q, Liu JT, Zhong YP et al (2002) The numeric simulations of water-bursting time-effect for faults in Zhaogezhuang coal mine, Kailuan, China. J China Coal Soc 27(5):512–516

Wu Q, Cui FP, Zhao SQ, Liu SQ, Zeng YF, Gu YW (2013) Type classification and main characteristics of mine water disasters. J China Coal Soc 38(4):561–565

Xia D (2014) Study on damage mechanics of soaking rock and application in mines containing water. PhD Diss. Northeastern University, China

Yang TH, Liu J, Zhu WC, Elsworthc D, Thamd LG, Tang CA (2007) A coupled flow-stress-damage model for groundwater outbursts from an underlying aquifer into mining excavations. Int J Rock Mech Min Sci 44(1):87–97

Yin SX, Zhang JC (2005) Impacts of karst paleo-sinkholes on mining and environment in northern China. Environ Geol 48(8):1077–1083

Yin SX, Wang SX, Wu Q (2004) Water inrush patterns and theoretic criteria of karstic collapse columns. Chin J Rock Mech Eng 23(6):964–968

Yin SX, Zhang JC, Liu DM (2015) A study of mine water inrushes by measurements of in situ stress and rock failures. Nat Hazards 79(3):1961–1979

Zhang JC (2005) Investigations of water inrushes from aquifers under coal seams. Int J Rock Mech Min Sci 42(3):350–360

Zhang JC, Shen BH (2004) Coal mining under aquifers in China: a case study. Int J Rock Mech Min Sci 41(4):629–639

Zhang HQ, He YN, Tang CA, Ahmad B, Han LJ (2009) Application of an improved flow-stress-damage model to the critically assessment of water inrush in a mine: a case study. Rock Mech Rock Eng 41(6):911–930

Zhang R, Jiang Z, Zhou H, Yang C, Xiao S (2014) Groundwater outbursts from faults above a confined aquifer in the coal mining. Nat Hazards 71(3):1861–1872

Zhang GM, Zhang Kai, Wang LJ, Wu Y (2015) Mechanism of water inrush and quicksand movement induced by a borehole and measures for prevention and remediation. B Eng Geol Environ 74(4):1395–1405

Zhu WC, Wei CH (2011) Numerical simulation on mining-induced water inrushes related to geologic structures using a damage-based hydromechanical model. Environ Earth Sci 62(1):43–54

Zuo JP, Peng SP, Li YJ, Chen ZH, Xie HP (2009) Investigation of karst collapse based on 3-D seismic technique and DDA method at Xieqiao coal mine, China. Int J Coal Geol 78(4):276–287